Journal of Computational Physics 228 (2009) 9092–9106

Contents lists available at ScienceDirect

Journal of Computational Physics

journal homepage: www.elsevier.com/locate/jcp

A real space split operator method for the Klein–Gordon equation

Matthias Ruf, Heiko Bauke *, Christoph H. Keitel

Max-Planck-Institut für Kernphysik, Saupfercheckweg 1, 69117 Heidelberg, Germany

ARTICLE INFO

Article history:
Received 5 June 2009
Received in revised form 7 September 2009
Accepted 8 September 2009
Available online 15 September 2009

PACS:
02.70.–c
03.65.Pm
02.70.Bf

Keywords:
Klein–Gordon equation
Split operator method
Numerical simulation

ABSTRACT

The Klein–Gordon equation is a Lorentz invariant equation of motion for spinless particles. We propose a real space split operator method for the solution of the time-dependent Klein–Gordon equation with arbitrary electromagnetic fields. Split operator methods for the Schrödinger equation and the Dirac equation typically operate alternately in real space and momentum space and, therefore, require the computation of a Fourier transform in each time step. However, the fact that the kinetic energy operator $\widehat{K}$ in the two-component representation of the Klein–Gordon equation is a nilpotent operator, that is $\widehat{K}^2 = 0$, allows us to implement the split operator method for the Klein–Gordon equation entirely in real space. Consequently, the split operator method for the Klein–Gordon equation does not require the computation of a Fourier transform and may be parallelized efficiently by domain decomposition.

1. Introduction

The quantum dynamics of high intensity laser matter interactions necessitate a relativistic treatment. Therefore, relativistic generalizations of the Schrödinger wave equation have to be applied, namely the Dirac equation for spin 1/2 particles or the Klein–Gordon equation for spinless particles. The derivation of analytical solutions of the Dirac equation or the Klein–Gordon equation requires sophisticated mathematical tools. Solutions of these equations with some specific potentials is presented, e.g. in [1–6]. However, many setups require numerical approaches [7–13], especially problems with time-dependent potentials. The numerical solution of the Dirac equation is computationally expensive and difficult to parallelize efficiently, which limits the systems to low spatial dimensionality or to low grid resolutions.

In this contribution, we will introduce a real space split operator method for the numerical solution of the Klein–Gordon equation with arbitrary electrodynamic potentials. Parallelization via domain decomposition leads to an almost linear speedup. Thus, for systems where the role of the electron's spin is insignificant the Klein–Gordon equation may be employed. Furthermore, we will present a parallel computer implementation of this method for one- and two-dimensional problems. The paper is organized as follows. In Section 2 we review the Klein–Gordon equation and in Section 3 we describe the split operator method, Section 4 gives an introduction to our numerical code and in Section 5 we show some applications of our Klein–Gordon solver.

* Corresponding author.
E-mail addresses: ruf@mpi-hd.mpg.de (M. Ruf), bauke@mpi-hd.mpg.de (H. Bauke), keitel@mpi-hd.mpg.de (C.H. Keitel).

0021-9991/$ - see front matter © 2009 Elsevier Inc. All rights reserved.
doi:10.1016/j.jcp.2009.09.012

2. The Klein–Gordon equation

The Klein–Gordon equation, a relativistic generalization of the Schrödinger wave equation, is an equation of motion for a scalar wave function $\varphi(\boldsymbol{x},t)$ [14]. It governs the behavior of a charged spinless particle with mass m and charge q moving under the effect of electrodynamic potentials $\boldsymbol{A}(\boldsymbol{x},t)$ and $\phi(\boldsymbol{x},t)$. Introducing the speed of light c, the Klein–Gordon equation reads

$$\left[\left(\mathrm{i}\hbar\frac{\partial}{\partial t}-q\phi(\boldsymbol{x},t)\right)^2-c^2\left(\frac{\hbar}{\mathrm{i}}\nabla-q\boldsymbol{A}(\boldsymbol{x},t)\right)^2-m^2c^4\right]\varphi(\boldsymbol{x},t)=0. \tag{1}$$

The discovery of the Klein–Gordon equation can be attributed to various physicists. Depending on who is credited, the equation is called Klein–Gordon equation, Klein–Fock–Gordon equation or Klein–Gordon–Schrödinger equation. See [15] for the history of the Klein–Gordon equation. Solutions $\varphi(\boldsymbol{x},t)$ of Eq. (1) satisfy the continuity equation

$$\frac{\partial\rho(\boldsymbol{x},t)}{\partial t}+\nabla\cdot\boldsymbol{j}(\boldsymbol{x},t)=0 \tag{2}$$

with the density

$$\rho(\boldsymbol{x},t)=\frac{\mathrm{i}\hbar}{2mc^2}\left[\varphi^*(\boldsymbol{x},t)\frac{\partial\varphi(\boldsymbol{x},t)}{\partial t}-\frac{\partial\varphi^*(\boldsymbol{x},t)}{\partial t}\varphi(\boldsymbol{x},t)\right]-\frac{q\phi(\boldsymbol{x},t)}{mc^2}\varphi^*(\boldsymbol{x},t)\varphi(\boldsymbol{x},t) \tag{3}$$

and the current

$$\boldsymbol{j}(\boldsymbol{x},t)=-\frac{\mathrm{i}\hbar}{2m}[\varphi^*(\boldsymbol{x},t)\nabla\varphi(\boldsymbol{x},t)-\nabla\varphi^*(\boldsymbol{x},t)\varphi(\boldsymbol{x},t)]-\frac{q\boldsymbol{A}(\boldsymbol{x},t)}{m}\varphi^*(\boldsymbol{x},t)\varphi(\boldsymbol{x},t), \tag{4}$$

where $\varphi^*(\boldsymbol{x},t)$ denotes the complex conjugate of $\varphi(\boldsymbol{x},t)$.

The Klein–Gordon Eq. (1) differs from the Schrödinger-type Hamiltonian form

$$\mathrm{i}\hbar\frac{\partial}{\partial t}\Psi(\boldsymbol{x},t)=\widehat{H}(t)\Psi(\boldsymbol{x},t) \tag{5}$$

of quantum mechanical equations of motion, the Klein–Gordon equation is of second order in time. Consequently, unique initial conditions require the specification of both the wave function and its time derivative. Furthermore, the density $\rho(\boldsymbol{x},t)$ is not positive definite. Therefore, $\rho(\boldsymbol{x},t)$ cannot be interpreted as a probability density and $\boldsymbol{j}(\boldsymbol{x},t)$ is not a probability density current.

However, these difficulties can be circumvented if one interprets the presence of a second order time derivative in the Klein–Gordon equation as a second degree of freedom of the wave function. The wave function's two degrees of freedom correspond to two different charge states and $q\rho(\boldsymbol{x},t)$ may be interpreted as a charge density and $q\boldsymbol{j}(\boldsymbol{x},t)$ as a charge current, see [2–5,14] for details. In Section 3.2 we will remind the reader how to transform the Klein–Gordon equation (1) into the Hamiltonian form (5).

3. The split operator method

The state of a quantum mechanical system is given by a wave function $\Psi(\boldsymbol{x},t)$ evolving in time t and space $\boldsymbol{x}$. Depending on the particle's spin, the complex function $\Psi(\boldsymbol{x},t)$ may be scalar or vector-valued. Its temporal evolution is governed by a Hermitian possibly time-dependent Hamilton operator $\widehat{H}(t)$ and Eq. (5). Using Dyson's time ordering operator $\widehat{T}$, the formal solution of (5) with the initial condition $\Psi(\boldsymbol{x},0)$ is given by

$$\Psi(\boldsymbol{x},t)=\widehat{U}(t,0)\Psi(\boldsymbol{x},0) \tag{6}$$

with the unitary time-evolution operator [16]

$$\widehat{U}(t_2,t_1)=\widehat{T}\exp\left(-\frac{\mathrm{i}}{\hbar}\int_{t_1}^{t_2}\widehat{H}(t')\,\mathrm{d}t'\right) \tag{7}$$

that effects the wave function's evolution from time t_1 to time t_2. For some highly symmetric quantum systems, analytic expressions of the time-evolution operator (7) can be calculated. However, investigations of many relevant quantum systems require numerical methods, e.g. the split operator method, which will be shortly described in the following paragraphs.

3.1. The general outline of the split operator method

Fleck et al. [17] introduced the split operator method as an explicit time-stepping scheme for the solution of the time-dependent scalar Maxwell's wave equation in Fresnel approximation. Shortly after Feit et al. [18] solved the Schrödinger equation with a time-independent Hamiltonian numerically by the split operator method, it became a standard tool for the propagation of quantum mechanical wave equations. Later, the method had been generalized to the Schrödinger equa-

tion with a time-dependent Hamiltonian [19] and it was applied to other equations, e.g. the Dirac equation [10–12,20], the time-dependent Gross–Pitaevskii equation [21], the non-linear Schrödinger equation [22], and the time-dependent Maxwell's equations for electromagnetic waves in random dielectric media [23].

It is very difficult to transfer the time-evolution operator (7) directly into a numerical scheme. The central idea of the split operator method is to approximate (7) by a product of operators that are diagonal either in real space or in momentum space. Let $\widehat{O}(t)$ denote some possibly time-dependent operator and define the operator

$$\widehat{U}_{\widehat{O}}(t_2,t_1,\delta)=\exp\left(-\delta\frac{\mathrm{i}}{\hbar}\int_{t_1}^{t_2}\widehat{O}(t')\,\mathrm{d}t'\right), \tag{8}$$

that depends on the times t_1 and t_2 and the auxiliary parameter δ. Furthermore, let us assume that the Hamiltonian is a sum of two other Hermitian operators

$$\widehat{H}(t)=\widehat{K}(t)+\widehat{V}(t), \tag{9}$$

e.g. the kinetic and the potential energy. Expanding $\widehat{U}(t+\Delta t,t)$ to the third order in Δt, the time-evolution operator (7) can be factorized as

$$\widehat{U}(t+\Delta t,t)=\exp\left(-\frac{\mathrm{i}}{\hbar}\int_t^{t+\Delta t}\widehat{H}(t')\,\mathrm{d}t'\right)+O(\Delta t^3)=\widehat{U}_{\widehat{V}}\left(t+\Delta t,t,\frac{1}{2}\right)\widehat{U}_{\widehat{K}}(t+\Delta t,t,1)\widehat{U}_{\widehat{V}}\left(t+\Delta t,t,\frac{1}{2}\right)+O(\Delta t^3). \tag{10}$$

Neglecting terms of order $O(\Delta t^3)$, Eq. (10) gives an explicit second order accurate time-stepping scheme for the propagation of the wave function

$$\Psi(\boldsymbol{x},t+\Delta t)=\widehat{U}_{\widehat{V}}\left(t+\Delta t,t,\frac{1}{2}\right)\widehat{U}_{\widehat{K}}(t+\Delta t,t,1)\widehat{U}_{\widehat{V}}\left(t+\Delta t,t,\frac{1}{2}\right)\Psi(\boldsymbol{x},t)+O(\Delta t^3). \tag{11}$$

This scheme translates the difficulty of calculating the action of operator (7) to the task of calculating the action of (8). In fact, for many quantum mechanical systems one can find a splitting (9) of the Hamiltonian $\widehat{H}(t)$ such that the operator $\widehat{U}_{\widehat{V}}(t+\Delta t,t,\delta)$ is diagonal in real space and $\widehat{U}_{\widehat{K}}(t+\Delta t,t,\delta)$ is diagonal in momentum space, respectively. Thus, the calculation of these operators becomes feasible in the appropriate space.

In a computer implementation of the split operator method, the wave function $\Psi(\boldsymbol{x},t)$ is discretized on a rectangular lattice of N points. The computational complexity of propagating the wave function from time t to time $t+\Delta t$ is dominated by the transformation of the wave function into momentum space and back into real space. If these transforms are accomplished by the fast Fourier transform the computation of an elementary step of the split operator method takes $O(N\log N)$ operations.

The split operator method introduces two kinds of numerical errors. One is due to the discretization of the spatial grid and appears in the calculation of $\widehat{U}_{\widehat{K}}(t+\Delta t,t,\delta)$ and the other is introduced by approximating the action of the time-evolution operator (7) by the splitting (10). However, the calculation of $\widehat{U}_{\widehat{V}}(t+\Delta t,t,\delta)$ and $\widehat{U}_{\widehat{K}}(t+\Delta t,t,\delta)$ is of infinite order of accuracy in Δt if carried out in spaces where $\widehat{V}$ and $\widehat{K}$ are diagonal. This means, there is no additional error in Δt induced by the calculation of $\widehat{U}_{\widehat{V}}(t+\Delta t,t,\delta)$ and $\widehat{U}_{\widehat{K}}(t+\Delta t,t,\delta)$.

Let us consider the Schrödinger equation for a particle of mass m and charge q in the electrodynamic potentials $\boldsymbol{A}(\boldsymbol{x},t)$ and $\phi(\boldsymbol{x},t)$

$$\mathrm{i}\hbar\frac{\partial\Psi(\boldsymbol{x},t)}{\partial t}=\widehat{H}(t)\Psi(\boldsymbol{x},t)=\left(\frac{1}{2m}\left(\frac{\hbar}{\mathrm{i}}\nabla-q\boldsymbol{A}(\boldsymbol{x},t)\right)^2+q\phi(\boldsymbol{x},t)\right)\Psi(\boldsymbol{x},t) \tag{12}$$

as an illustrative example. In the so-called dipole approximation it is assumed that the vector potential is homogeneous, i.e., $\boldsymbol{A}(\boldsymbol{x},t)=\boldsymbol{A}(t)$. Splitting the Hamiltonian (12) into the two operators

$$\widehat{K}(t)=-\frac{\hbar^2}{2m}\nabla^2-\frac{\hbar q}{\mathrm{i}m}\boldsymbol{A}(t)\cdot\nabla+\frac{q^2\boldsymbol{A}(t)^2}{2m}, \tag{13a}$$

$$\widehat{V}(t)=q\phi(\boldsymbol{x},t) \tag{13b}$$

separates spatial dependent parts from spatial derivatives, which makes the operator $\widehat{U}_{\widehat{V}}(t+\Delta t,t,\delta)$ diagonal in real space and $\widehat{U}_{\widehat{K}}(t+\Delta t,t,\delta)$ diagonal in momentum space, respectively.

Note that in our example, it is crucial that the vector potential $\boldsymbol{A}(t)$ does not depend on the spatial coordinate $\boldsymbol{x}$. The expansion of the Hamiltonian of the Schrödinger equation (12) for a particle in an arbitrary vector potential $\boldsymbol{A}(\boldsymbol{x},t)$ contains the term $(\mathrm{i}q\hbar/m)\boldsymbol{A}(\boldsymbol{x},t)\cdot\nabla$, that is spatially dependent and contains spatial derivatives, too, coupling momentum and coordinate space. Thus, the operator $\widehat{K}(t)$ cannot always be diagonalized by a Fourier transform and the operator $\widehat{U}_{\widehat{K}}(t_1,t_2,\delta)$ is not generally diagonal in momentum space. The operator $\widehat{U}_{\widehat{K}}(t+\Delta t,t,\delta)$ is diagonal in momentum space only if the vector potential $\boldsymbol{A}(\boldsymbol{x},t)$ commutes with the canonical momentum operator $-\mathrm{i}\hbar\nabla$, as for example in the case of the vector potential of a linearly polarized plane wave $\boldsymbol{A}(\boldsymbol{x},t)=(A_x(z,t),0,0)$ [20]. The calculation of the action of the operator $\widehat{U}_{\widehat{K}}(t+\Delta t,t,\delta)$ for the Schrödinger Eq. (12) with arbitrary vector potentials $\boldsymbol{A}(\boldsymbol{x},t)$ requires special methods, for example:

- Diagonalizing $\widehat{K}(t)$ makes the computation of $\widehat{U}_{\widehat{K}}(t+\Delta t,t,\delta)$ trivial. However, diagonalizing $\widehat{K}(t)$ at each time step is computationally very expensive.
- One may expand $\widehat{U}_{\widehat{K}}(t+\Delta t,t,\delta)$ into a Padé approximant and approximate partial derivatives by finite differences, which results in implicit Crank–Nicolson-like algorithms [24]. This approach is less accurate than computing $\widehat{U}_{\widehat{K}}(t+\Delta t,t,\delta)$ in the diagonal space of $\widehat{K}$. It requires the solution of (at least one) linear system of equations at each time step and will not scale well in parallel computations.
- Real space product formulas [25,26] allow to compute the action of $\widehat{U}_{\widehat{K}}(t+\Delta t,t,\delta)$ in real space similar to our approach to the Klein–Gordon equation. This requires an additional splitting of $\widehat{U}_{\widehat{K}}(t+\Delta t,t,\delta)$ that introduces an additional source of numerical error. Real space product formulas, however, are attractive for parallelization [27].

The operator $\widehat{U}_{\widehat{K}}(t+\Delta t,t,\delta)$ is not diagonal in momentum space because the Schrödinger equation is of second order in the spatial coordinates. For quantum wave equations that are only of first order in the spatial coordinates as the Dirac equation [11,12], however, a Fourier transform diagonalizes $\widehat{U}_{\widehat{K}}(t+\Delta t,t,\delta)$.

3.2. The Klein–Gordon equation in Hamiltonian form

In this contribution, we will apply the split operator method to the Klein–Gordon Eq. (1). This form of the Klein–Gordon equation is of second order in time and, therefore, differs from the usual Hamiltonian form (5) of quantum mechanical equations of motion and it is not appropriate for the split operator method. However, it is possible to transform (1) into a Hamiltonian form (5) [14] by introducing a two-component wave function

$$\Psi(\boldsymbol{x},t)=\begin{pmatrix}\Psi_1(\boldsymbol{x},t)\\ \Psi_2(\boldsymbol{x},t)\end{pmatrix}=\begin{pmatrix}\frac{1}{2}\left(\varphi(\boldsymbol{x},t)+\frac{1}{mc^2}\left(\mathrm{i}\hbar\frac{\partial}{\partial t}-q\phi(\boldsymbol{x},t)\right)\varphi(\boldsymbol{x},t)\right)\\ \frac{1}{2}\left(\varphi(\boldsymbol{x},t)-\frac{1}{mc^2}\left(\mathrm{i}\hbar\frac{\partial}{\partial t}-q\phi(\boldsymbol{x},t)\right)\varphi(\boldsymbol{x},t)\right)\end{pmatrix}. \tag{14}$$

The equation of motion for this new wave function reads

$$\mathrm{i}\hbar\frac{\partial\Psi(\boldsymbol{x},t)}{\partial t}=\widehat{H}(t)\Psi(\boldsymbol{x},t)=\left(\frac{\tau_3+\mathrm{i}\tau_2}{2m}\left(\frac{\hbar}{\mathrm{i}}\nabla-q\boldsymbol{A}(\boldsymbol{x},t)\right)^2+q\phi(\boldsymbol{x},t)+\tau_3mc^2\right)\Psi(\boldsymbol{x},t) \tag{15}$$

and has the desired Hamiltonian form (5). The wave function's components are related by the Pauli matrices τ_2 and τ_3

$$\tau_1=\begin{pmatrix}0&1\\1&0\end{pmatrix},\quad \tau_2=\begin{pmatrix}0&-\mathrm{i}\\ \mathrm{i}&0\end{pmatrix},\quad \tau_3=\begin{pmatrix}1&0\\0&-1\end{pmatrix}. \tag{16}$$

The Pauli matrices are complex Hermitian unitary matrices that obey the Pauli algebra

$$\tau_i\tau_j=\mathrm{i}\epsilon_{i,j,k}\tau_k+\delta_{i,j}, \tag{17a}$$
$$[\tau_i,\tau_j]=2\mathrm{i}\epsilon_{i,j,k}\tau_k, \tag{17b}$$
$$\{\tau_i,\tau_j\}=2\delta_{i,j}, \tag{17c}$$

with $i,j,k\in\{1,2,3\}$ and where $\epsilon_{i,j,k}$ denotes the permutation symbol (also known as the Levi-Civita symbol) and $\delta_{i,j}$ is the Kronecker delta. The density (3) as a function of the two-component wave function $\Psi(\boldsymbol{x},t)$ is given by

$$\rho(\boldsymbol{x},t)=\Psi^*(\boldsymbol{x},t)\tau_3\Psi(\boldsymbol{x},t). \tag{18}$$

One should note that the Klein–Gordon–Hamiltonian (15) is not Hermitian ($\widehat{H}(t)\neq\widehat{H}(t)^\dagger$) because $\tau_3+\mathrm{i}\tau_2$ is not a Hermitian matrix and, consequently, the time-evolution operator of the Klein–Gordon–Hamiltonian is not unitary ($\widehat{U}^{-1}\neq\widehat{U}^\dagger$). However, the Klein–Gordon–Hamiltonian is a τ_3-pseudo-Hermitian operator and its time-evolution operator is τ_3-pseudo-unitary [28,29]. A linear operator $\widehat{H}$ acting in a Hilbert space $\mathcal{H}$ is called $\hat{\eta}$-pseudo-Hermitian if there is a Hermitian operator $\hat{\eta}$ such that

$$\hat{\eta}^{-1}\widehat{H}^\dagger\hat{\eta}=\widehat{H}. \tag{19}$$

The operator $\widehat{H}^\#=\hat{\eta}^{-1}\widehat{H}^\dagger\hat{\eta}$ is named the $\hat{\eta}$-pseudo-adjoint of $\widehat{H}$. Let $\Psi_1,\Psi_2\in\mathcal{H}$ and $\langle\Psi_1|\Psi_2\rangle$ the inner product in $\mathcal{H}$. The operator $\hat{\eta}$ defines the pseudo-inner-product

$$\langle\Psi_1|\Psi_2\rangle_{\hat{\eta}}=\langle\Psi_1|\hat{\eta}\Psi_2\rangle. \tag{20}$$

The pseudo-inner-product (20) is conjugate symmetric, linear in its second argument, but in contrast to usual inner-products not necessarily positive-definite. The operator $\widehat{H}$ is Hermitian with respect to the pseudo-inner-product (20)

$$\langle\widehat{H}\Psi_1|\Psi_2\rangle_{\hat{\eta}}=\langle\Psi_1|\widehat{H}\Psi_2\rangle_{\hat{\eta}}. \tag{21}$$

A linear invertible operator $\widehat{U}$ acting on $\mathcal{H}$ is called $\hat{\eta}$-pseudo-unitary if

$$\hat{\eta}^{-1}\widehat{U}^\dagger\hat{\eta}=\widehat{U}^{-1}. \tag{22}$$

The inner product (20) is invariant under $\hat{\eta}$-pseudo-unitary transforms

$$\langle \Psi_1 | \Psi_2 \rangle_{\hat{\eta}} = \langle \widehat{U} \Psi_1 | \widehat{U} \Psi_2 \rangle_{\hat{\eta}}. \tag{23}$$

Expectation values $\langle O \rangle$ of observables having operator $\widehat{O}$ are computed by the pseudo-inner-product (20), that is

$$\langle O \rangle = \langle \Psi_1 | \widehat{O} \Psi_1 \rangle_{\hat{\eta}}. \tag{24}$$

3.3. A split operator method for the Klein–Gordon equation

In Section 3.1 we stated that there does not exist a splitting (9) of the Hamiltonian of the Schrödinger Eq. (12) with arbitrary electrodynamic potentials $\boldsymbol{A}(\boldsymbol{x}, t)$ and $\phi(\boldsymbol{x}, t)$ such that the operators $\widehat{U}_{\widehat{V}}(t + \Delta t, t, \delta)$ and $\widehat{U}_{\widehat{K}}(t + \Delta t, t, \delta)$ are diagonal in real space or in momentum space, respectively. The Klein–Gordon equation (15) has a structure that is very similar to the Schrödinger Eq. (12). In fact, there is no appropriate splitting (9) of the Klein–Gordon Hamiltonian (15) such that the operators $\widehat{U}_{\widehat{V}}(t + \Delta t, t, \delta)$ and $\widehat{U}_{\widehat{K}}(t + \Delta t, t, \delta)$ are diagonal in real space or in momentum space, respectively. However, as we will show, it is possible to apply the split operator method to the Klein–Gordon equation (15) without making $\widehat{U}_{\widehat{K}}(t + \Delta t, t, \delta)$ diagonal in momentum space.

We split the Klein–Gordon Hamiltonian (15) into a kinetic energy part

$$\widehat{K}(\boldsymbol{x}, t) = \frac{\tau_3 + \mathrm{i}\tau_2}{2m} \left(\frac{\hbar}{\mathrm{i}} \nabla - q\boldsymbol{A}(\boldsymbol{x}, t) \right)^2 \tag{25a}$$

and a potential energy part

$$\widehat{V}(\boldsymbol{x}, t) = q\phi(\boldsymbol{x}, t) + \tau_3 mc^2. \tag{25b}$$

With this splitting and the standard representation of the Pauli matrices (16), the operator $\widehat{U}_{\widehat{V}}(t + \Delta t, t, \delta)$ is diagonal in real space

$$\begin{aligned} \widehat{U}_{\widehat{V}}(t + \Delta t, t, \delta) \Psi(\boldsymbol{x}, t) &= \exp\left(-\delta \frac{\mathrm{i}}{\hbar} \int_t^{t+\Delta t} \widehat{V}(\boldsymbol{x}, t')\, \mathrm{d}t' \right) \Psi(\boldsymbol{x}, t) = \exp\left(-\delta \frac{\mathrm{i}}{\hbar} \int_t^{t+\Delta t} q\phi(\boldsymbol{x}, t') + \tau_3 mc^2\, \mathrm{d}t' \right) \Psi(\boldsymbol{x}, t) \\ &= \begin{pmatrix} \exp\left(-\delta \frac{\mathrm{i}}{\hbar} \int_t^{t+\Delta t} q\phi(\boldsymbol{x}, t') + mc^2\, \mathrm{d}t' \right) \Psi_1(\boldsymbol{x}, t) \\ \exp\left(-\delta \frac{\mathrm{i}}{\hbar} \int_t^{t+\Delta t} q\phi(\boldsymbol{x}, t') - mc^2\, \mathrm{d}t' \right) \Psi_2(\boldsymbol{x}, t) \end{pmatrix}. \end{aligned} \tag{26}$$

The operator $\widehat{U}_{\widehat{K}}(t + \Delta t, t, \delta)$ is not diagonal neither in real space nor in momentum space. We calculate the action of operator $\widehat{U}_{\widehat{K}}(t + \Delta t, t, \delta)$ on $\Psi(\boldsymbol{x}, t)$ in real space by the Taylor series of the exponential function

$$\begin{aligned} \widehat{U}_{\widehat{K}}(t + \Delta t, t, \delta) \Psi(\boldsymbol{x}, t) &= \exp\left(-\delta \frac{\mathrm{i}}{\hbar} \int_t^{t+\Delta t} \widehat{K}(\boldsymbol{x}, t')\, \mathrm{d}t' \right) \Psi(\boldsymbol{x}, t) \\ &= \sum_{j=0}^{\infty} \frac{1}{j!} \left[-\delta \frac{\mathrm{i}}{\hbar} \int_t^{t+\Delta t} \frac{\tau_3 + \mathrm{i}\tau_2}{2m} \left(\frac{\hbar}{\mathrm{i}} \nabla - q\boldsymbol{A}(\boldsymbol{x}, t') \right)^2 \mathrm{d}t' \right]^j \Psi(\boldsymbol{x}, t) \\ &= \sum_{j=0}^{\infty} \frac{(\tau_3 + \mathrm{i}\tau_2)^j}{j!} \left[\frac{-\delta \mathrm{i}}{2m\hbar} \int_t^{t+\Delta t} \left(\frac{\hbar}{\mathrm{i}} \nabla - q\boldsymbol{A}(\boldsymbol{x}, t') \right)^2 \mathrm{d}t' \right]^j \Psi(\boldsymbol{x}, t). \end{aligned} \tag{27}$$

The infinite series (27) comprises spatial derivatives of $\Psi(\boldsymbol{x}, t)$ of arbitrary high order. However, from (17) it follows that the operator $(\tau_3 + \mathrm{i}\tau_2)$ is a nilpotent operator, that is, $(\tau_3 + \mathrm{i}\tau_2)^2 = 0$. Therefore, the kinetic energy operator $\widehat{K}(\boldsymbol{x}, t)$ is nilpotent, too, and the series (27) reduces to

$$\widehat{U}_{\widehat{K}}(t + \Delta t, t, \delta) \Psi(\boldsymbol{x}, t) = \Psi(\boldsymbol{x}, t) - (\tau_3 + \mathrm{i}\tau_2) \frac{\delta \mathrm{i}}{2m\hbar} \int_t^{t+\Delta t} \left(\frac{\hbar}{\mathrm{i}} \nabla - q\boldsymbol{A}(\boldsymbol{x}, t') \right)^2 \Psi(\boldsymbol{x}, t)\, \mathrm{d}t'. \tag{28}$$

Thus, the features of the Pauli algebra (17) and the nilpotency of the kinetic energy operator $\widehat{K}(\boldsymbol{x}, t)$ allow us to calculate the action of the exponential operator (27) on $\Psi(\boldsymbol{x}, t)$ by first and second order derivatives of $\Psi(\boldsymbol{x}, t)$ only. One should note that for the free time-dependent Maxwell's equations one can devise a similar operator splitting where one of the operators is nilpotent [23].

Introducing the quantities

$$c_1 = \frac{\delta \mathrm{i} \Delta t \hbar}{2m}, \tag{29a}$$

$$c_2 = \frac{\delta q}{m} \int_t^{t+\Delta t} \boldsymbol{A}(\boldsymbol{x}, t')\, \mathrm{d}t', \tag{29b}$$

$$c_3 = \int_t^{t+\Delta t} \frac{\delta q}{2m} \nabla \cdot \boldsymbol{A}(\boldsymbol{x}, t') - \frac{\delta \mathrm{i} q^2}{2m\hbar} \boldsymbol{A}(\boldsymbol{x}, t')^2\, \mathrm{d}t', \tag{29c}$$

and

$$\psi(\boldsymbol{x},t) = \Psi_1(\boldsymbol{x},t) + \Psi_2(\boldsymbol{x},t), \tag{29d}$$

and taking advantage of the standard representation (16) of the Pauli matrices, where

$$\tau_3 + \mathrm{i}\tau_2 = \begin{pmatrix} 1 & 1 \\ -1 & -1 \end{pmatrix}, \tag{30}$$

the operator (28) may be written in the compact form

$$\widehat{U}_{\widehat{K}}(t+\Delta t,t,\delta)\begin{pmatrix}\Psi_1(\boldsymbol{x},t)\\ \Psi_2(\boldsymbol{x},t)\end{pmatrix} = \begin{pmatrix}\Psi_1(\boldsymbol{x},t) + (c_1\nabla^2\psi(\boldsymbol{x},t) + c_2\cdot\nabla\psi(\boldsymbol{x},t) + c_3\psi(\boldsymbol{x},t))\\ \Psi_2(\boldsymbol{x},t) - (c_1\nabla^2\psi(\boldsymbol{x},t) + c_2\cdot\nabla\psi(\boldsymbol{x},t) + c_3\psi(\boldsymbol{x},t))\end{pmatrix}. \tag{31}$$

In a numerical implementation of the split operator method, the wave function $\Psi(\boldsymbol{x},t)$ is discretized on a rectangular grid. It is propagated from time t to time $t+\Delta t$ by (11) with (26) and (28). First and second order derivatives on the right hand side of (28) are approximated by a finite difference scheme. The integrals (29b) and (29c) can be approximated numerically if not given analytically. The computation of (29c) simplifies considerably if the electrodynamic potentials are given in Coulomb gauge, viz. $\nabla\cdot\boldsymbol{A}(\boldsymbol{x},t) = 0$.

Finally, we would like to note that our real space split operator method may be generalized easily to higher orders of accuracy [30–32], provided that the electromagnetic potentials do not depend on time. For time-dependent potentials, time ordering has to be taken into account [19].

4. The Klein–Gordon code in a nutshell

We have implemented a computer program that solves the time-dependent Klein–Gordon equation in one or two spatial dimensions by taking advantage of the split operator method as outlined in Section 3. In contrast to traditional split operator-schemes that operate alternately in real space and momentum space, our split operator-scheme for the Klein–Gordon equation acts exclusively in real space. Thus, the application of (11) does not require the computation of a Fourier transform. This has several computational advantages.

- There are no restrictions on the electromagnetic potentials as opposed to other second order quantum wave equations.
- An elementary step of the split operator method for the Klein–Gordon equation takes only $O(N)$ operations, while a fast Fourier transform would require $O(N\log N)$ operations, where N denotes the number of spatial grid points.
- The split operator method for the Klein–Gordon equation can be parallelized efficiently on shared memory and distributed memory parallel computers by domain decomposition with a small communication overhead. Parallelization is required, because relativistic propagation methods suffer from the problem, that the time steps Δt have to be considerably smaller compared to non-relativistic propagation schemes.
- The discrete Fourier transform requires an evenly spaced spatial grid, our real space split operator method allows for unevenly spaced spatial grids giving more flexibility.

In the following, we present the main features of our numerical implementation of the Klein–Gordon theory.

4.1. Finite differences

For the approximation of the partial derivatives in (31), we implemented various finite difference schemes, ranging from three point up to nine point formulas. In all following numerical simulations, a five point scheme has been employed. Calculation of the partial derivatives based on the pseudo-spectral-element methods [33] or the finite-element discrete-variable representation [27] allow for higher accuracy but have not yet implemented.

4.2. Parallelization

The propagation of a Klein–Gordon wave function may be parallelized on shared and distributed memory parallel computers by a one- or two-dimensional grid decomposition depending on the system's dimensionality. The grid is split into smaller ones, which are propagated individually. The application of the operator $\widehat{U}_{\widehat{V}}(t+\Delta t,t,\delta)$ is an "embarrassingly" parallel task, this means, the action of $\widehat{U}_{\widehat{V}}(t+\Delta t,t,\delta)$ on $\Psi(\boldsymbol{x},t)$ may be separated into several parallel tasks without communication overhead. However, the parallel application of the operator $\widehat{U}_{\widehat{K}}(t+\Delta t,t,\delta)$ requires the exchange of data points on the surface of the sub-grids due to the calculation of derivatives via finite differences. Therefore, neighboring sub-grids have to exchange the content of their boundary region at each time step. This was implemented by MPI (Message Passing Interface) routines [34,35].

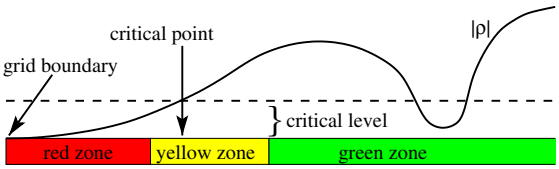

Fig. 1. Schematic representation of the grid adjustment. The black solid curve represents the magnitude of the density $|\rho|$, for a typical example shape, and the black dashed line corresponds to the critical level. The critical point is the position of the intersection of the former two, which lies nearest to the boundary. The grid is adjusted depending on the location of the critical point compared to the grid's red, yellow and green zones. In the example shown, the critical point lies in the yellow zone, meaning that the distance to the grid boundary has an acceptable size on this side. (For interpretation of the references to color in this figure legend, the reader is referred to the web version of this article.)

4.3. Absorbing boundary

During the propagation, parts of the wave packet may hit the boundary introducing reflection effects. To avoid these undesirable boundary effects, an absorbing boundary of width d is employed. After n successive time steps, the wave function is damped to zero on the boundary by multiplying the wave function with the damping function

$$f(x,y) = g(x - x_l, d)g(-(x - x_r), d)g(y - y_l, d)g(-(y - y_r), d), \tag{32}$$

where the smooth function $g(x,d) \in C^\infty$ is defined as

$$g(x,d) = \left(1 + \exp\left(-2\tan\left(\frac{\pi}{2} + \frac{\pi x}{d}\right)\right)\right)^{-1} \Theta(x)\Theta(d - x) + \Theta(x - d), \tag{33}$$

utilizing the Heaviside step function $\Theta(x)$. The function $f(x,y)$ is zero everywhere outside the grid $[x_l, x_r] \times [y_l, y_r]$ and one in $[x_l + d, x_r - d] \times [y_l + d, y_r - d]$. In the intersection of these domains $f(x,y)$ grows continuously and smoothly from zero to one. In order to avoid reflections at the boundary we recommend to ensure that

$$n\,\Delta t\, c < d. \tag{34}$$

4.4. Grid adjustment

A crucial step to gain a highly efficient numerical code is to adjust the underlying grid to the propagated wave function in order to keep the grid as small as possible. It should follow the movement of the main part of the wave packet. It should also take into account the possibility that the wave packet changes its shape, becoming broader or narrower during the propagation. Adjusting the grid to a minimal required size will save valuable computing time.

We adjust the computational grid successively after a specified number of time steps. The grid adjusting method is shown schematically in Fig. 1 and works as follows. It operates by shrinking or extending the rectangular grid at each of its edges separately. At the edge under consideration, three regions are introduced; named red, yellow, and green zone. We calculate the magnitude of the density (the density itself could be negative) and call regions significant where the magnitude of the density exceeds a pre-defined critical level. A critical point is a point in a significant region that has the smallest distance to the edge under consideration. The grid has an acceptable size if the critical points lie in the yellow zone. However, if a critical point lies in the red zone, it is too close to the boundary. Therefore the grid is enlarged at this side such that critical points lie in the middle of the yellow zone. On the contrary, if critical points lie in the green zone, they are too far from the boundary, and the grid is too large at the investigated side. Thus, it can be shrunk till the critical points lie again in the middle of the yellow zone.

5. Numerical results

In order to illustrate the strengths and capabilities of our Klein–Gordon code, we are going to present several instructive examples featuring signatures of relativistic quantum dynamics. The first example considers the evolution of a free Gaussian wave packet. In the next example, we demonstrate the propagation of an initially free particle under the influence of a plane-wave laser field. Further examples consider the motion along a circular orbit in a two-dimensional harmonic potential and scattering on a potential step, which leads to the Klein paradox.

Numerical simulations are performed in atomic units. In atomic units, length is measured in terms of the Bohr radius $x_{\text{a.u.}} = a_0$, mass and charge are given in units of the electron's mass $m_{\text{a.u.}} = m_e$ and the absolute value $q_{\text{a.u.}} = e$ of its charge, respectively, the angular momentum is measured in units of the Planck constant divided by $2\pi, L_{\text{a.u.}} = h/(2\pi) = \hbar$. Atomic units of physical quantities with other dimensions than length, mass, charge or angular momentum can be expressed as products of $x_{\text{a.u.}}, m_{\text{a.u.}}, q_{\text{a.u.}}$ and $L_{\text{a.u.}}$, see Table 1. The speed of light in the atomic unit system constitutes $c \approx 137.036\, v_{\text{a.u.}}$.

5.1. Evolution of a free Gaussian wave packet

A free particle at rest is implemented in our code as a wave packet having a Gaussian momentum distribution. For non-vanishing initial mean momentum $\bar{\boldsymbol{p}}$, this wave packet is Lorentz boosted along $\bar{\boldsymbol{p}}$. Thus, the free particle is represented by a

Table 1
Elementary units of the atomic unit system for some physical quantities.

Quantity	Elementary unit of the atomic unit system
Length	$x_{\text{a.u.}} = a_0 = 4\pi\varepsilon_0\hbar^2/(m_e e^2)$
Mass	$m_{\text{a.u.}} = m_e$
Charge	$q_{\text{a.u.}} = e$
Angular momentum	$L_{\text{a.u.}} = h/(2\pi) = \hbar$
Time	$t_{\text{a.u.}} = m_{\text{a.u.}} x_{\text{a.u.}}^2 / L_{\text{a.u.}}$
Velocity	$v_{\text{a.u.}} = L_{\text{a.u.}}/(m_{\text{a.u.}} x_{\text{a.u.}})$
Momentum	$p_{\text{a.u.}} = L_{\text{a.u.}}/x_{\text{a.u.}}$
Electric field strength	$E_{\text{a.u.}} = L_{\text{a.u.}}^2/(m_{\text{a.u.}} x_{\text{a.u.}}^3 q_{\text{a.u.}})$

Gaussian wave packet in its rest frame. Wave packets $\Psi_{\bar{\boldsymbol{p}}}^{(+)}$ and $\Psi_{\bar{\boldsymbol{p}}}^{(-)}$ may be formed by integrating over eigen-states of the free Klein–Gordon–Hamiltonian with either positive ($\Psi_{\bar{\boldsymbol{p}}}^{(+)}$) or negative ($\Psi_{\bar{\boldsymbol{p}}}^{(-)}$) energy. Explicitly we have

$$\Psi_{\bar{\boldsymbol{p}}}^{(\pm)}(\boldsymbol{x},t) = \mathcal{N}\int \frac{\sqrt{E'-c\boldsymbol{\beta}\bar{\boldsymbol{p}}}}{E'}\exp\left(-\frac{\boldsymbol{p}(\boldsymbol{p}')^2}{2\sigma^2}\right)\begin{pmatrix} mc^2 \pm E' \\ mc^2 \mp E' \end{pmatrix}\exp\left(\frac{\mathrm{i}}{\hbar}(\boldsymbol{p}'\cdot\boldsymbol{x} \mp E't)\right)\mathrm{d}^3p', \tag{35}$$

where $E' = c\sqrt{(mc)^2+\boldsymbol{p}'^2}$ is the relativistic energy, σ is the initial width in momentum space, $\boldsymbol{\beta} = \bar{\boldsymbol{p}}/\sqrt{m^2c^2+\bar{\boldsymbol{p}}^2}$, and $\mathcal{N}$ is a normalization factor. The momentum $\boldsymbol{p}(\boldsymbol{p}')$ follows from the inverse Lorentz transformation Λ^{-1}

$$\begin{pmatrix} E/c \\ \boldsymbol{p} \end{pmatrix} = \Lambda^{-1}\begin{pmatrix} E'/c \\ \boldsymbol{p}' \end{pmatrix}, \tag{36}$$

where the unprimed (primed) quantities refer to the rest (laboratory) frame of the particle. The shape of the wave packet in the laboratory frame is Lorentz contracted along the direction of the initial momentum.

We consider propagation in one and two dimensions with an initial width $\sigma = 400p_{\text{a.u.}}$, an initial momentum $|\bar{\boldsymbol{p}}| = 100p_{\text{a.u.}}$ along the x-axis, and positive energy. This corresponds to a rather narrow initial wave packet. For this parameter set the evolution of the charge density of a relativistic Klein–Gordon wave packet differs significantly from the non-relativistic theory of the Schrödinger equation, where a Gaussian wave packet broadens but remains its Gaussian shape for all times and the maximum of the charge density travels with the same speed as the motion of the center of charge does.

The evolution of the charge density (3) of one- and two-dimensional relativistic Klein–Gordon wave packets is illustrated in Figs. 2 and 3. Note that we present all charge densities in this paper at a logarithmic scale to reveal the structure of the wave function even at small densities, this, however, requires to plot the absolute value of the charge distribution. Although the initial state consists of a Gaussian superposition of positive-energy plane-wave states only, the charge density of the initial wave packet is non-Gaussian and becomes negative in the outer region, not visible in Fig. 2. The position of the initial charge density's maximum corresponds to the initial center of charge. The wave packet's center of charge moves in accordance with classical predictions with velocity $|\bar{\boldsymbol{p}}|/(m\sqrt{1+\bar{\boldsymbol{p}}^2/(mc)^2}) \approx 81\,v_{\text{a.u.}}$ along the x-axis. However, at later times shock fronts emerge traveling approximately with the speed of light into all directions. Maxima of the charge density no longer coincide with the center of charge. In the two-dimensional system, a ring structure evolves with an inherent asymmetry with respect to the direction of the initial momentum. See [36] for an investigation of similar relativistic effects.

The reason for the appearance of a partly negative charge density and the strange evolution behavior of the wave packet is provided by the following arguments. As a consequence of the uncertainty principle and the possibility of pair creation, a relativistic quantum theory does not allow to measure the position of a particle with arbitrary high precision. This is

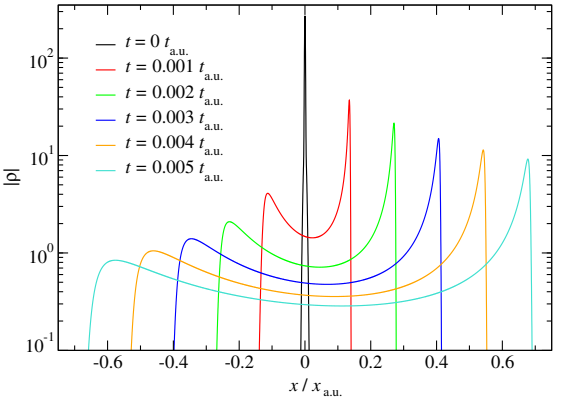

Fig. 2. Time evolution of a free narrow positive-energy Gaussian wave packet in one dimension with initial momentum $\bar{p} = 100p_{\text{a.u.}}$ and a width in momentum space of $\sigma = 400p_{\text{a.u.}}$. The plot shows charge densities on a logarithmic scale. The wave packet splits into two shock fronts traveling into opposite directions.

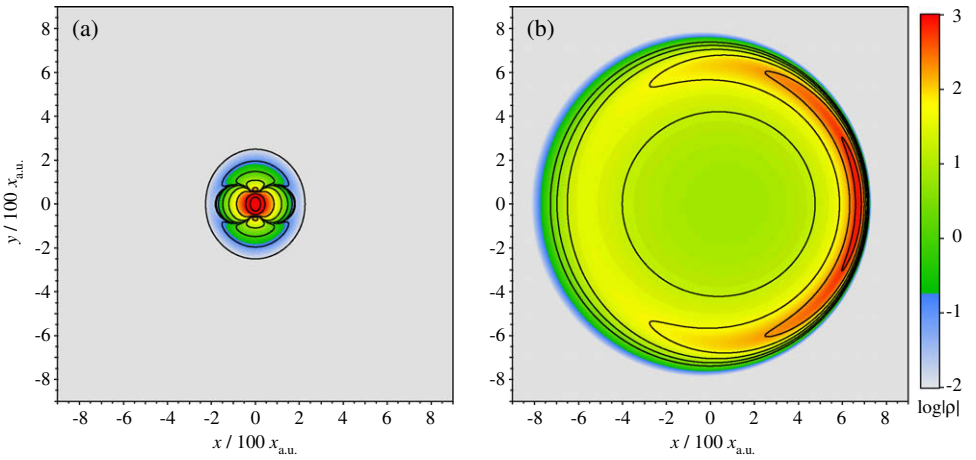

Fig. 3. Time evolution of a narrow positive-energy Gaussian wave packet in two dimensions with initial momentum $\bar{\boldsymbol{p}} = (100p_{\text{a.u.}}, 0p_{\text{a.u.}})$ and a width in momentum space of $\sigma = 400p_{\text{a.u.}}$. The plots picture the logarithm of the magnitude of the density. Part (a) shows the initial wave packet at $t = 0t_{\text{a.u.}}$, where the outer part around the main peak exhibits a negative charge density. The contour lines start at -2 with a spacing of 1. Part (b) presents the charge density at $t = 0.0005t_{\text{a.u.}}$. The contour lines start at 0.5 with a spacing of 0.25. The charge density develops "shock waves" in an asymmetric ring structure.

reflected in our case by the appearance of a negative charge density if the width in position space becomes smaller than a critical lengths Δx_c given by the Compton wave length of the particle, $\Delta x_c \sim \lambda_C = h/mc$. This critical length corresponds to a momentum uncertainty of $\Delta p_c \sim mc$, which corresponds to the lowest bound of pair creation. The approach to measure the position of a particle to a higher accuracy than Δx_c, would lead inevitably to particle–antiparticle pair creation, rendering the position measurement meaningless [37].

The deformation of the wave packet during the propagation from the usual Gaussian shape is due to the finite speed of light [38]. In order to keep the Gaussian shape, the portions with high momentum would have to move faster than the speed of light. This is of course impossible. Therefore, shock fronts build up which move approximately with the speed of light. In the one-dimensional simulation, these shock fronts correspond to the two parts traveling in opposite directions, whereas for the two-dimensional simulation the shock front occurs as the outward traveling ring.

These two examples of an extremely narrow Gaussian wave packet show rather striking qualitative differences between the non-relativistic and relativistic theory. We point out, however, that for a moderate width of the initial Gaussian distribution shock fronts do not build up and wave packets spread similar to the non-relativistic theory.

The free wave packet is one of the few systems where a closed analytic solution is known, see Eq. (35). Thus, it allows us to test the numerical accuracy of our Klein–Gordon split operator method by comparing the numerical propagated wave function $\Psi(\boldsymbol{x}, t)$ from the analytical one $\tilde{\Psi}(\boldsymbol{x}, t)$, given by (35). For this purpose we define the deviation in magnitude of the upper and lower component as

$$\varepsilon_{1,2}(\boldsymbol{x}, t) = \|\tilde{\Psi}_{1,2}(\boldsymbol{x}, t)| - |\Psi_{1,2}(\boldsymbol{x}, t)\|. \tag{37}$$

The two lines in Fig. 4 show the maximal deviation $\max_{\boldsymbol{x}} \varepsilon_{1,2}(\boldsymbol{x}, t)$ at different propagation times for the same wave packet as in Fig. 2. The maximal numerical error increases linearly in time. The inset of Fig. 4 corresponds to the deviation for the largest time shown in Fig. 2. Due to the extreme wave packet parameters, the absolute deviation is rather large. However, one should note, that the maximal deviation appears at the shock front, where the first and second derivatives of the wave function exhibit large values. At the shock front they are approximately four orders of magnitude larger as compared to other regions. Relative errors are, however, in the few percent range.

5.2. Motion in a relativistic laser field

During recent years, there has been an enormous progress in laser technology and relativistic effects become important for investigations of laser-matter interactions. A charged particle in a laser field represents a first step in this direction. A free electron in an external laser field enters the relativistic regime when the relativistic laser parameter $\xi = E_0/(mc\omega)$ approaches or exceeds unity. Here, ω and E_0 denote the laser circular frequency and field strength, respectively.

We chose a linearly polarized plane-wave laser pulse, where the polarization axis corresponds to the y-direction and the pulse propagates from the left to the right in the x-direction. Introducing the laser phase $\eta = \omega(x/c - t)$, the vector potential is given by

$$\boldsymbol{A}(\eta) = \boldsymbol{e}_y \frac{E_0}{\omega} \cos(\eta) g(\eta). \tag{38}$$

The pulse shape function $g(\eta)$ consists of a single cycle $\sin^2$-turn-on followed by a single cycle constant plateau region and a single cycle $\sin^2$-turn-off. In Fig. 5 we took $\omega = 5/t_{\text{a.u.}}$ and $E_0 = 300E_{\text{a.u.}}$, which correspond to a wave length of about 9 nm

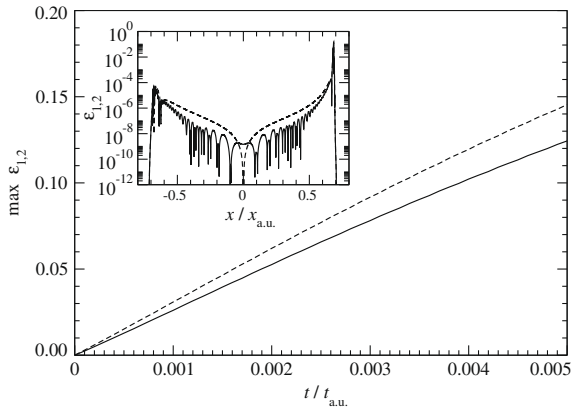

Fig. 4. Comparison between the analytical $\Psi(\boldsymbol{x},t)$ and the numerical $\bar{\Psi}(\boldsymbol{x},t)$ solution of the free wave packet from Fig. 2. Plotted is the maximal deviation in magnitude $\max_{\boldsymbol{x}}\varepsilon(\boldsymbol{x},t) = \max_{\boldsymbol{x}}||\Psi_{1,2}(\boldsymbol{x},t)| - |\bar{\Psi}_{1,2}(\boldsymbol{x},t)||$ of the first (dashed line) and of the second (solid line) component of the wave function as a function of time. The inset shows the deviation $\varepsilon(\boldsymbol{x},t)$ at $t = 0.005 t_{\text{a.u.}}$. One should note, that the maximal deviation appears at the shock front traveling to the right, and that it is approximately four orders of magnitude larger as compared to other regions.

and an intensity of 3×10^{21} W/cm^2. With these field parameters, we enter the weakly relativistic regime $\xi = 0.44 < 1$ and the signature of the relativistic Lorentz force becomes apparent. This field is applied to a free positive-energy Gaussian wave packet initially at rest at the origin. The black curve depicts the center-of-charge trajectory and displays the typical zig-zag motion. The particle oscillates along the polarization axis with an amplitude $\Delta y = qE_0/(m\omega^2)$ and moves a distance $\Delta x = \pi q^2 E_0^2/(2cm^2\omega^3)$ per cycle along the propagation direction [39,40]. The motion perpendicular to the laser's electric field component is due to the magnetic component of the Lorentz force, acting on the particle and pushing it along the laser propagation direction.

The Klein–Gordon equation is an excellent approximation to the Dirac equation for systems, where the particle's dynamics is not affected by the particle's spin degree of freedom or if the spin plays a negligible role. The scattering of a laser driven electron at ions, as given in Fig. 6, is such a system where the spin can be neglected. This example was chosen to allow a direct comparison with a former calculation employing the Dirac theory [41]. Here, an initial free Gaussian wave packet is propagated under the influence of a relativistic laser field with field parameters $E_0 = 50E_{\text{a.u.}}$, $\omega = 1/t_{\text{a.u.}}$, corresponding to a wave length of about 46 nm and an intensity of 9×10^{19} W/cm^2, and scatters at two additional ions modeled by softcore potentials

$$\phi(\boldsymbol{r}) = \sum_{i=1}^{2} \frac{-Ze}{4\pi\varepsilon_0\sqrt{|\boldsymbol{r} - \boldsymbol{r}_{\text{ion},i}|^2 + a}}, \tag{39}$$

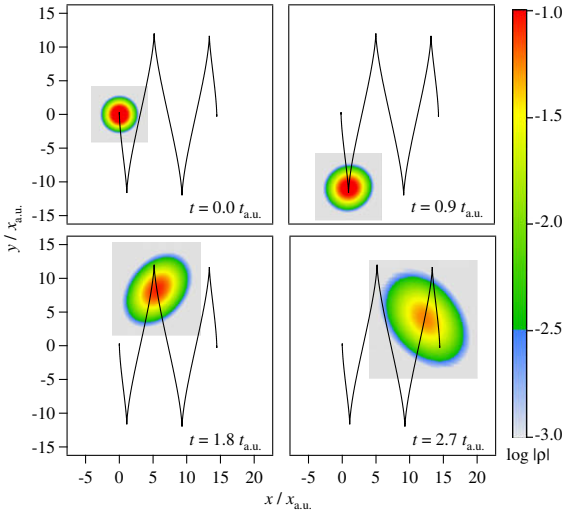

Fig. 5. Propagation of a free positive-energy Gaussian wave packet under the influence of an intense laser pulse traveling into the x-direction ($E_0 = 300E_{\text{a.u.}}$, $\omega = 5/t_{\text{a.u.}}$). The black curve denotes the position expectation value, corresponding to the center of charge. Note the grid movement along the particle trajectory and the adjustment in size in accordance to the growing wave packet.

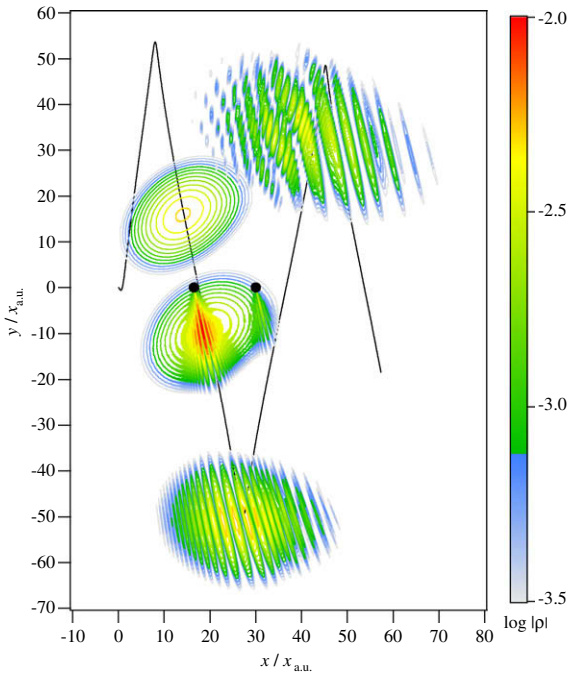

Fig. 6. Time evolution of a wave packet in a laser field at various times ($t = 7.645t_{\text{a.u.}}$, $t = 8.195t_{\text{a.u.}}$, $t = 9.495t_{\text{a.u.}}$, $t = 12.095t_{\text{a.u.}}$), scattering at two nuclei modeled by softcore potentials (39). The two nuclei are indicated by the black dots. Contour plots show the charge density, the continuous line pictures the center of charge trajectory.

with $a = (0.1x_{\text{a.u.}})^2$, and $Z = 50$. The black circles in Fig. 6 represent the two ions which are located at $\boldsymbol{r}_{\text{ion},1} = (16.5x_{\text{a.u.}}, 0)$ and $\boldsymbol{r}_{\text{ion},2} = (30x_{\text{a.u.}}, 0)$. The scattering process causes a complex diffraction pattern. On the level of resolution in Fig. 6 the diffraction patterns of Dirac wave packets [41] cannot be distinguished from the Klein–Gordon wave packets in Fig. 6, compare Fig. 6 with Fig. 1 in [41] which shows the same scattering process with the same set of parameters in the framework of the Dirac equation. Thus, the spin degree of freedom does not affect the wave-packet's dynamics in this example.

In general, one can estimate the spin-degree's impact on the wave-packet's dynamics by comparing spin terms to non-spin terms in the expansion of the Dirac Hamiltonian by a Foldy–Wouthuysen transformation [5]. In this way, one can show, for example, that the spin plays a negligible role for unbounded particles in strong laser fields as long as $\max[\hbar\omega\xi/(mc^2), Zme^5\omega/(64\hbar^3c^2\pi^2\varepsilon_0^3E)] \ll 1$ and $\omega \ll \sqrt{ceE_0/\hbar}$ [42]. For strongly bound states spin orbit coupling may become important and alters the dynamics significantly [43,44].

5.3. Harmonic oscillator

Our next example features a particle on a circular orbit in a two-dimensional harmonic oscillator potential

$$q\phi(\boldsymbol{x}, t) = \frac{1}{2}m\omega^2|\boldsymbol{x}|^2. \tag{40}$$

In order that the wave packet travels on a circular orbit, the initial position $\boldsymbol{x}_0$ and the initial momentum $\boldsymbol{p}_0$ of the particle have to be chosen suitably. These parameters can be calculated classically taking into account relativistic effects. In a classical calculation, a particle's motion in a two- or three-dimensional harmonic potential can be reduced to a one-dimensional motion in an effective potential

$$V_{\text{eff}}(r) = \frac{1}{2}m\omega^2r^2 + \frac{L^2}{2mr^2} \tag{41}$$

with $r = |\boldsymbol{x}|$ and $L = |\boldsymbol{x}_0 \times \boldsymbol{p}_0|$ denoting the angular momentum as a function of the initial position and the initial momentum. The trajectory will be circular if the effective potential attains its minimum at the initial radius $r_0 = |\boldsymbol{x}_0|$ and $\boldsymbol{x}_0$ and $\boldsymbol{p}_0$ are perpendicular. The condition

$$\left.\frac{\mathrm{d}V_{\text{eff}}(r)}{\mathrm{d}r}\right|_{r=r_0} = 0 \tag{42}$$

gives the relation $r_0 = |\boldsymbol{p}_0|/(m\omega)$ that has to be fulfilled by the initial position and the initial momentum for a circular orbit.

An effective potential may also be introduced in the relativistic case

$$V_{\text{eff}}(r) = \frac{1}{2}m\omega^2 r^2 + \sqrt{m^2c^4 + \frac{c^2L^2}{r^2}}. \tag{43}$$

From the minimum of this effective potential, one can extract the relativistically modified radius of the circular orbit

$$r_0 = \frac{|\boldsymbol{p}_0|}{m\omega}\left(1 + \left(\frac{|\boldsymbol{p}_0|}{mc}\right)^2\right)^{-1/4} = \frac{|\boldsymbol{p}_0|}{m\omega}\left[1 - \frac{1}{4}\left(\frac{|\boldsymbol{p}_0|}{mc}\right)^2 + \frac{5}{32}\left(\frac{|\boldsymbol{p}_0|}{mc}\right)^4 + O\left(\left(\frac{|\boldsymbol{p}_0|}{mc}\right)^6\right)\right]. \tag{44}$$

The relativistic reduction of the radius becomes apparent if the initial momentum is sufficiently large, that is $|\boldsymbol{p}_0| > mc$. For the parameters $\omega = 20/t_{\text{a.u.}}$ and $|\boldsymbol{p}_0| = 150p_{\text{a.u.}}$ the non-relativistic radius equals $r_0 = 7.5x_{\text{a.u.}}$, while the relativistic calculation yields $r_0 \approx 6.16x_{\text{a.u.}}$. This is confirmed by our numerical propagation shown in Fig. 7. The center of charge describes a circle with a radius predicted by Eq. (44).

5.4. Potential step and the Klein paradox

The investigation of particles incident upon a potential step leads to the well-known Klein paradox [45–48]. This phenomenon, which is not known in non-relativistic quantum mechanics, is connected to the existence of negative energy solutions. These, however, represent a major problem in the one-particle picture, because transitions between positive and negative energy states are related to the phenomenon of pair creation. Thus, whenever such transitions occur one has to leave the one-particle picture when interpreting the results. In early days the Klein paradox was considered as just a "Gedankenexperiment". However, it has been demonstrated [49] that graphene provides an effective medium where the Klein paradox may be tested experimentally.

In order to avoid numerical instabilities, we implemented a smoothed version of the potential step given by

$$\phi(\boldsymbol{r}) = \frac{\phi_0}{2}\left(\tanh\frac{x}{\Delta x} + 1\right), \tag{45}$$

where Δx corresponds to the width of the rising region, and ϕ_0 defines the height of the potential step. The qualitative dynamics of the scattering process depends on the potential height ϕ_0. For $\phi_0 < 2mc^2$ the particle is reflected or transmitted analogous to the non-relativistic Schrödinger theory and the potential is called subcritical. However, for $\phi_0 > 2mc^2$ pair creation occurs and therefore, the potential is called supercritical.

We consider a positive-energy particle approaching the potential step from the left. For a subcritical potential, the behavior is similar to the non-relativistic case. If the energy of the incoming wave packet is less than the potential step, the wave packet is reflected. If the energy exceeds the potential step height, the wave packet splits into a reflected and a transmitted part. The angle between the x-axis and the direction in which the transmitted part of the wave packet propagates follows from the continuity of the wave function and the energy conservation at the potential step. It is given by

$$\tan\theta = \frac{p_{0,y}}{mc}\left[\left(\sqrt{1 + \left(\frac{\boldsymbol{p}_0}{mc}\right)^2} - \frac{\phi_0}{mc^2}\right)^2 - \left(\frac{p_{0,y}}{mc}\right)^2 - 1\right]^{-1/2}, \tag{46}$$

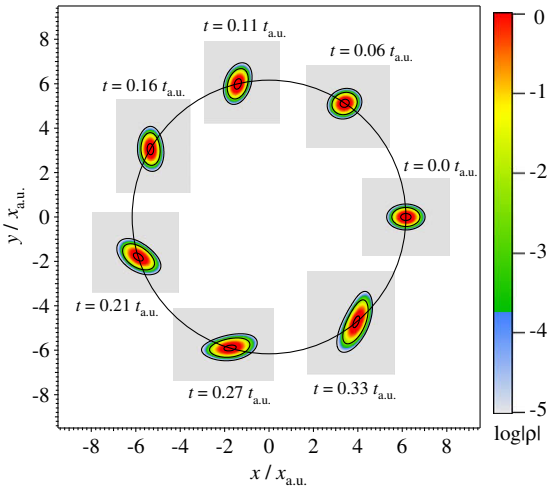

Fig. 7. Time evolution of a wave packet in a harmonic oscillator potential (40) with $\omega = 20/t_{\text{a.u.}}$. The initial parameters are chosen in such a way, that the particle undergoes a circular motion. This is also an instructive example of the grid adjustment.

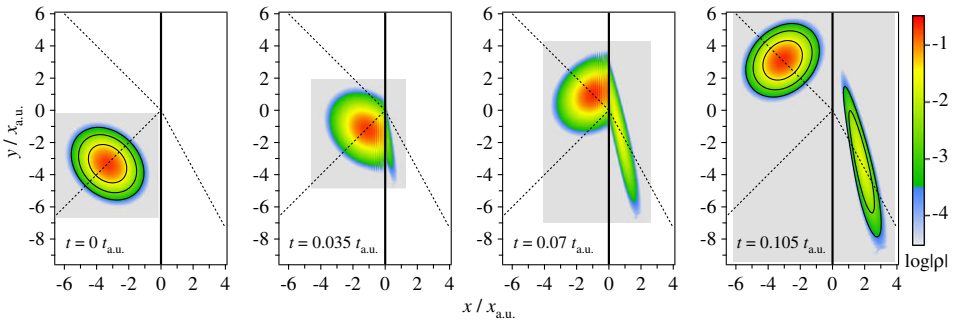

Fig. 8. Time evolution of a wave packet approaching a supercritical potential step at $x = 0$ indicated by a solid black line. The initial momentum is low leading to the Klein paradox. Although the main part of the wave packet is reflected at the potential step, a small component propagates into the forbidden region ($x > 0$) having negative density.

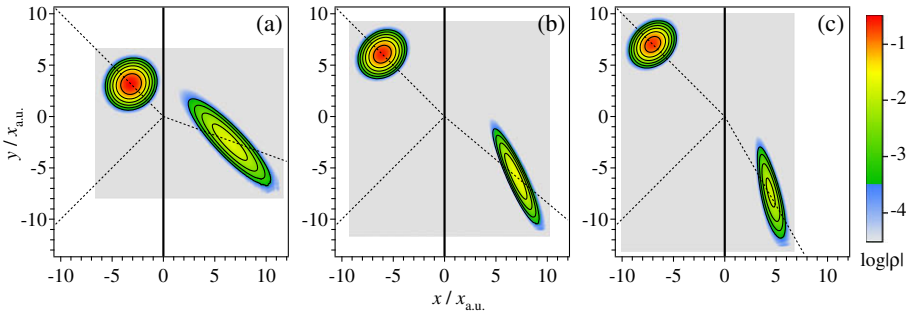

Fig. 9. Klein paradox for a particle impinging a potential step of height $\phi_0 = 2.5mc^2$ under an angle of 45° with different initial momenta $\boldsymbol{p}_0 = (p, p)$: (a) $p = 0.333\,mc,\ \theta = 20°$; (b) $p = 0.505\,mc,\ \theta = 40°$; (c) $p = 0.582\,mc,\ \theta = 60°$. A part of the wave function propagates into the normally forbidden region ($x > 0$) to the right along the direction θ predicted by (46).

where $\boldsymbol{p}_0 = (p_{x,0}, p_{y,0})$ is the initial momentum. For subcritical fields Eq. (46) yields real values only for energies which are higher than $\phi_0 + mc^2$.

We turn now to the more interesting case of a supercritical potential. Here a new situation arises if the energy of the incoming particle is sufficiently low ($mc^2 < E < \phi_0 - mc^2$). In addition to a reflected part, a portion of the wave packet propagates further into the (non-relativistically) "forbidden" region with an energy smaller than the step height. This phenomenon is known as the Klein paradox [45–47]. An example of this is shown in Fig. 8 for $\phi_0 = 2.5mc^2, \Delta x = 0.0025x_{\text{a.u.}}$, and an initial momentum of $\boldsymbol{p}_0/mc = (0.5874, 0.5874)$. Although the main part of the wave packet is reflected at the potential step, a small component propagates into the "forbidden" region, having negative density, and consists in fact of negative energy states. So both negative and positive-energy states are involved in this regime and one is forced to leave the one-particle picture.

The usual textbook argument [2–5] states, that the incoming particle is totally reflected at the potential step. However, during this reflection a particle-antiparticle pair is created additionally. So, the portion of the wave packet which propagates into the forbidden region to the right is interpreted as the created antiparticle. Taking into account the fermionic character of particles a completely different explanation of the Klein paradox in the Dirac theory was given recently [50,51], where this transition into negative energy states is explained as a suppression of an intrinsic pair creation process, inherent to a supercritical potential step.

Eq. (46) agrees with the numerically found propagation directions even for the case of the Klein paradox; the negative branch of the outermost square has to be chosen to take the negative energy into account. An example of this is given in Fig. 9 for the same field parameters as in Fig. 8.

6. Computational performance

In order to test the parallel efficiency of our parallel Klein–Gordon code, we examined how the computing time of the parallel code scales with the number of processes. For this purpose, we propagated a free Gaussian wave packet on a grid of size 1024×1024 over a fixed time interval varying the number of processes and measured the computing time. The speedup factor s_n is defined by $s_n = t_1/t_n$, where t_n denotes the running time of the program for n processes.

An ideal speedup grows proportionally to the number of processes, $s_n = n$. In practice, however, speedup grows sub-linearly, because parallel processes have to coordinate their work by explicit message exchange. The larger the ratio

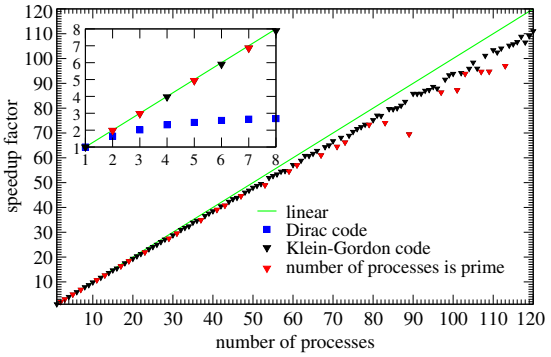

Fig. 10. Speedup factor versus the number of processes for the Klein–Gordon equation split operator code and a Dirac equation split operator code [12]. The green solid curve represents the ideal linear speedup. Red triangles indicate that the number of processes is prime. In this case the computational grid has to be divided into narrow stripes causing a unfavorable ratio between the total number of grid points and the number of grid points at the boundary of the sub-grids. Consequently, the communication overhead becomes exceptionally large and the speedup is reduced if the number of processes is prime. (For interpretation of the references to color in this figure legend, the reader is referred to the web version of this article.)

of message exchange time to actual computing time the larger the deviation from an ideal speedup. This ratio depends on the kind of computational problem as well as on the computing hardware, especial the communication network.

We performed benchmark tests on a Cluster of Dual Core AMD Opteron CPUs and an InfiniBand Double Data Rate interconnect with 5 GBit/s bandwidth. Fig. 10 shows the speedup results for different numbers of processes. The speedup profile follows approximately the ideal linear curve. However, the relative portion of the communication overhead grows with the number of processes resulting in a notable deviation from linear speedup. If the number of processes is prime, then the deviation from linear speedup is particularly large, because in this case the computational grid has to be broken into small stripes which causes a higher amount of communication overhead.

The inset of Fig. 10 presents the same data as the main figure does for small numbers of processes and compares it to the speedup profile of a state of the art split operator code for the Dirac equation [12]. For the Dirac equation, the split operator method requires successive transformations of the wave function from real space to momentum space and back again by a fast Fourier transform. This task can be parallelized. However, it demands a rather complex communication patter that limits the speedup. Consequently, the Dirac split operator code shows considerable sub-linear speedup as indicated by the blue squares in the inset of Fig. 10. Performance measurements for the solution of the Dirac equation have been taken on a Quad Core Intel Xeon system with two CPUs (a total of eight cores).

7. Conclusions and outlook

We have introduced a real space split operator method for the solution of the time-dependent Klein–Gordon equation with arbitrary electromagnetic fields. This method does not require consecutive transformations from real space to momentum space and vice versa and, therefore, allows for an efficient parallelization by domain decomposition. The split operator method for the Klein–Gordon equation was implemented in a parallel MPI program. We demonstrated that this method is capable of simulating a wide range of physical problems of relativistic light matter interactions. Its parallel computational performance is superior to the parallel performance of Dirac solvers, that are limited by the poor parallel performance of the fast Fourier transform.

Because of its computational advantages we suggest the solution of the Klein–Gordon equation in the numerical investigation of relativistic light matter interaction problems in place of the Dirac equation [8,10–12] if spin effects are not important. It would be interesting to apply our real space split operator method to other problems of relativistic quantum dynamics. The real space split operator method may be extended by allowing unevenly spaced grids or combining it with pseudo-spectral-element methods [33] or the finite-element discrete-variable representation [27].

References

[1] V.G. Bagrov, D. Gitman, Exact solutions of relativistic wave equations, Mathematics and its Applications, vol. 39, Springer, 1990.
[2] F. Gross, Relativistic Quantum Mechanics and Field Theory, Wiley & Sons, 1999.
[3] P. Strange, Relativistic Quantum Mechanics With Applications in Condensed Matter and Atomic Physics, Cambridge University Press, 1998.
[4] F. Schwabl, Advanced Quantum Mechanics, fourth ed., Springer, 2008.
[5] A. Wachter, Relativistic Quantum Mechanics, first ed., Springer, 2009.
[6] F. Ehlotzky, K. Krajewska, J.Z. Kamiński, Fundamental processes of quantum electrodynamics in laser fields of relativistic power, Reports on Progress in Physics 72 (4) (2009) 1–32, doi:10.1088/0034-4885/72/4/046401.
[7] N.J. Kylstra, A.M. Ermolaev, C.J. Joachain, Relativistic effects in the time evolution of a one-dimensional model atom in an intense laser field, Journal of Physics B: Atomic, Molecular and Optical Physics 30 (1997) L449–L460, doi:10.1088/0953-4075/30/13/001.
[8] U.W. Rathe, C.H. Keitel, M. Protopapas, P.L. Knight, Intense laser-atom dynamics with the two-dimensional Dirac equation, Journal of Physics B 30 (15) (1997) L531–L539, doi:10.1088/0953-4075/30/15/004.

[9] R. Taïeb, V. Véniard, A. Maquet, Signature of relativistic effects in atom–laser interactions at ultrahigh intensities, Physical Review Letters 81 (14) (1998) 2882–2885, doi:10.1103/PhysRevLett.81.2882.
[10] J.W. Braun, Q. Su, R. Grobe, Numerical approach to solve the time-dependent Dirac equation, Physical Review A 59 (1) (1999) 604–612, doi:10.1103/PhysRevA.59.604.
[11] G.R. Mocken, C.H. Keitel, Quantum dynamics of relativistic electrons, Journal of Computational Physics 199 (2) (2004) 558–588, doi:10.1016/j.jcp.2004.02.020.
[12] G.R. Mocken, C.H. Keitel, FFT-split-operator code for solving the Dirac equation in $2+1$ dimensions, Computer Physics Communications 178 (11) (2008) 868–882, doi:10.1016/j.cpc.2008.01.042.
[13] S. SelstØ, E. Lindroth, J. Bengtsson, Solution of the Dirac equation for hydrogenlike systems exposed to intense electromagnetic pulses, Physical Review A 79 (4) (2009) 043418, doi:10.1103/PhysRevA.79.043418.
[14] H. Feshbach, F. Villars, Elementary relativistic wave mechanics of spin 0 and spin 1/2 particles, Reviews of Modern Physics 30 (1) (1958) 24–45, doi:10.1103/RevModPhys.30.24.
[15] H. Kragh, Equation with the many fathers. The Klein–Gordon equation in 1926, American Journal of Physics 52 (11) (1984) 1024–1033, doi:10.1119/1.13782.
[16] P. Pechukas, J.C. Light, On the exponential form of time–displacement operators in quantum mechanics, The Journal of Chemical Physics 44 (10) (1966) 3897–3912, doi:10.1063/1.1726550.
[17] J.A. Fleck, J.R. Morris, M.D. Feit, Time-dependent propagation of high energy laser beams through the atmosphere, Applied Physics 10 (2) (1976) 129–160.
[18] M.D. Feit, J.A. Fleck Jr., A. Steiger, Solution of the Schrödinger equation by a spectral method, Journal of Computational Physics 47 (3) (1982) 412–433, doi:10.1016/0021-9991(82)90091-2.
[19] A.D. Bandrauk, H. Shen, Exponential split operator methods for solving coupled time-dependent Schrödinger equations, Journal of Chemical Physics 99 (2) (1993) 1185–1193, doi:10.1063/1.465362.
[20] S.X. Hu, C.H. Keitel, Dynamics of multiply charged ions in intense laser fields, Physical Review A 63 (5) (2001) 053402, doi:10.1103/PhysRevA.63.053402.
[21] J. Javanainen, J. Ruostekoski, Symbolic calculation in development of algorithms: split-step methods for the Gross–Pitaevskii equation, Journal of Physics A 39 (12) (2006) L179–L184, doi:10.1088/0305-4470/39/12/L02.
[22] G.M. Muslu, H.A. Erbay, Higher-order split-step Fourier schemes for the generalized nonlinear Schrödinger equation, Mathematics and Computers in Simulation 67 (6) (2005) 581–595, doi:10.1016/j.matcom.2004.08.002.
[23] W. Harshawardhan, Q. Su, R. Grobe, Numerical solution of the time-dependent maxwell's equations for random dielectric media, Physical Review E 62 (6) (2000) 8705–8712, doi:10.1103/PhysRevE.62.8705.
[24] A. Goldberg, H.M. Schey, J.L. Schwartz, Computer-generated motion pictures of one-dimensional quantum-mechanical transmission and reflection phenomena, American Journal of Physics 35 (3) (1967) 177–186, doi:10.1119/1.1973991.
[25] L. Collins, J.D. Kress, R.B. Walker, Excitation and ionization of molecules by a single-mode laser field using a time-dependent approach, Computer Physics Communications 114 (1–3) (1998) 15–26, doi:10.1016/S0010-4655(98)00055-1.
[26] B.I. Schneider, L.A. Collins, The discrete variable method for the solution of the time-dependent Schrödinger equation, Journal of Non-Crystalline Solids 351 (18) (2005) 1551–1558, doi:10.1016/j.jnoncrysol.2005.03.028.
[27] B.I. Schneider, L.A. Collins, S.X. Hu, Parallel solver for the time-dependent linear and nonlinear Schrödinger equation, Physical Review E 73 (3) (2006) 036708, doi:10.1103/PhysRevE.73.036708.
[28] A. Mostafazadeh, Pseudo-hermitian quantum mechanics, 2008, arXiv:0810.5643.
[29] A. Mostafazadeh, Pseudounitary operators and pseudounitary quantum dynamics, Journal of Mathematical Physics 45 (3) (2004) 932–946, doi:10.1063/1.1646448.
[30] H. Yoshida, Construction of higher order symplectic integrators, Physics Letters A 150 (5–7) (1990) 262–268, doi:10.1016/0375-9601(90)90092-3.
[31] M. Suzuki, General theory of higher-order decomposition of exponential operators and symplectic integrators, Physics Letters A 165 (5–6) (1992) 387–395, doi:10.1016/0375-9601(92)90335-J.
[32] A.D. Bandrauk, E. Dehghanian, H. Lu, Complex integration steps in decomposition of quantum exponential evolution operators, Chemical Physics Letters 419 (5) (2006) 346–350, doi:10.1016/j.cplett.2005.12.006.
[33] J.P. Boyd, Chebyshev and Fourier Spectral Methods, second ed., Dover, 1999.
[34] M. Snir, W. Gropp, MPI: The Complete Reference, MIT Press, 1998.
[35] H. Bauke, S. Mertens, Cluster Computing, Springer, 2006.
[36] Q. Su, B. Smetanko, R. Grobe, Relativistic suppression of wave packet spreading, Optics Express 2 (7) (1998) 277–281.
[37] L. Landau, E.M. Lifschitz, Quantum Electrodynamics, second ed., Butterworth-Heinemann, 1982.
[38] B. Thaller, Advanced Visual Quantum Mechanics, Springer, 2004.
[39] Y.I. Salamin, F.H.M. Faisal, Harmonic generation by superintense light scattering from relativistic electrons, Physical Review A 54 (5) (1996) 4383–4395, doi:10.1103/PhysRevA.54.4383.
[40] R.E. Wooten, J.H. Macek, Solutions of relativistic Newton's equations for nonconstant fields, American Journal of Physics 72 (8) (2004) 998–1001, doi:10.1119/1.1759357.
[41] G.R. Mocken, C.H. Keitel, Quantum signatures in laser-driven relativistic multiple scattering, Physical Review Letters 91 (17) (2003) 173202, doi:10.1103/PhysRevLett.91.173202.
[42] M. Klaiber, K.Z. Hatsagortsyan, C.H. Keitel, Above-threshold ionization beyond the dipole approximation, Physical Review A 71 (3) (2005) 033408, doi:10.1103/PhysRevA.71.033408.
[43] S.X. Hu, C.H. Keitel, Spin signatures in intense laser–ion interaction, Physical Review Letters 83 (23) (1999) 4709–4712, doi:10.1103/PhysRevLett.83.4709.
[44] M.W. Walser, D.J. Urbach, K.Z. Hatsagortsyan, S.X. Hu, C.H. Keitel, Spin and radiation in intense laser fields, Physical Review A 65 (4) (2002) 043410, doi:10.1103/PhysRevA.65.043410.
[45] O. Klein, Die Reflektion von Elektronen an einem Potentialsprung nach der relativistischen Dynamik von Dirac, Zeitschrift für Physik 53 (3–4) (1929) 157–165, doi:10.1007/BF01339716.
[46] F. Sauter, Über das Verhalten eines Elektrons im homogenen elektrischen Feld nach der relativistischen Theorie Diracs, Zeitschrift für Physik 69 (11–12) (1931) 742–764, doi:10.1007/BF01339461.
[47] F. Sauter, Zum "Kleinschen Paradoxon", Zeitschrift für Physik 73 (7–8) (1931) 547–552, doi:10.1007/BF01349862.
[48] A. Calogeracos, N. Dombey, History and physics of the Klein paradox, Contemporary Physics 40 (5) (1999) 313–321.
[49] M.I. Katsnelson, K.S. Novoselov, A.K. Geim, Chiral tunnelling and the Klein paradox in graphene, Nature Physics 2 (2006) 620–625. http://dx.doi.org/doi:10.1038/nphys384.
[50] P. Krekora, Q. Su, R. Grobe, Klein paradox in spatial and temporal resolution, Physical Review Letters 92 (4) (2004) 040406, doi:10.1103/PhysRevLett.92.040406.
[51] P. Krekora, Q. Su, R. Grobe, Transitions into the negative-energy Dirac continuum, Physical Review A 70 (5) (2004) 054101, doi:10.1103/PhysRevA.70.054101.